1-1-2018

Stoichiometry dependent inhibition of rat α3β4 nicotinic acetylcholine receptor by the ribbon isomer of α-conotoxin AuIB

Xiaosa Wu
University of Queensland

Han Shen Tae
University of Wollongong, hstae@uow.edu.au

Yen-Hua Huang
University of Queensland

David J. Adams
University of Wollongong, djadams@uow.edu.au

David J. Craik
University of Queensland

See next page for additional authors

Stoichiometry dependent inhibition of rat α3β4 nicotinic acetylcholine receptor by the ribbon isomer of α-conotoxin AuIB

Abstract

The ribbon isomer of α-conotoxin AuIB has 10-fold greater potency than the wild-type globular isomer at inhibiting nicotinic acetylcholine receptors (nAChRs) in rat parasympathetic neurons, and unlike its globular isoform, ribbon AuIB only targets a specific stoichiometry of the α3β4 nAChR subtype. Previous electrophysiological recordings of AuIB indicated that ribbon AuIB binds to the α3(+)α3(−) interface within the nAChR extracellular domain, which is displayed by the $(\alpha3)_3(\beta4)_2$ stoichiometry but not by $(\alpha3)_2(\beta4)_3$. This specificity for a particular stoichiometry is remarkable and suggests that ribbon isoforms of α-conotoxins might have great potential in drug design. In this study, we investigated the binding mode and structure-activity relationships of ribbon AuIB using a combination of molecular modeling and electrophysiology recording to determine the features that underpin its selectivity. An alanine scan showed that positions 4 and 9 of ribbon AuIB are the main determinants of the interaction with $(\alpha3)_3(\beta4)_2$ nAChR. Our computational models indicate that the first loop of ribbon AuIB binds in the "aromatic box" of the acetylcholine orthosteric binding site, similar to that of globular AuIB. In contrast, the second loop and the termini of the ribbon isomer have different orientations and interactions in the binding sites to those of the globular isomer. The structure-activity relationships reported herein should be useful to design peptides displaying a ribbon α-conotoxin scaffold for inhibition of nAChR subtypes that have hitherto been difficult to selectively target.

Disciplines

Medicine and Health Sciences

Publication Details

Wu, X., Tae, H., Huang, Y., Adams, D. J., Craik, D. J. & Kaas, Q. (2018). Stoichiometry dependent inhibition of rat α3β4 nicotinic acetylcholine receptor by the ribbon isomer of α-conotoxin AuIB. Biochemical Pharmacology, 155 288-297.

Authors

Xiaosa Wu, Han Shen Tae, Yen-Hua Huang, David J. Adams, David J. Craik, and Quentin Kaas

Stoichiometry dependent inhibition of rat α3β4 nicotinic acetylcholine receptor by the ribbon isomer of α-conotoxin AuIB

Xiaosa Wu[a], Han-Shen Tae[b], Yen-Hua Huang[a], David J. Adams[b], David J. Craik[a,*] and Quentin Kaas[a,*]

[a] Institute for Molecular Bioscience, The University of Queensland, Brisbane, Queensland 4072, Australia.

[b] Illawarra Health and Medical Research Institute (IHMRI), The University of Wollongong, Wollongong, New South Wales 2522, Australia.

Correspondence:

David J. Craik, Institute for Molecular Bioscience, The University of Queensland, Brisbane, Queensland 4072, Australia. Telephone: 61-7-33462019; FAX: 61-7-33462101; Email: d.craik@imb.uq.edu.au

Quentin Kaas, Institute for Molecular Bioscience, The University of Queensland, Brisbane, Queensland 4072, Australia. Telephone: 61-7-33462021; FAX: 61-7-33462101; Email: q.kaas@imb.uq.edu.au

ABSTRACT

The ribbon isomer of α-conotoxin AuIB has 10-fold greater potency than the wild-type globular isomer at inhibiting nicotinic acetylcholine receptors (nAChRs) in rat parasympathetic neurons, and unlike its globular isoform, ribbon AuIB only targets a specific stoichiometry of the α3β4 nAChR subtype. Previous electrophysiological recordings of AuIB indicated that ribbon AuIB binds to the α3(+)α3(−) interface within the nAChR extracellular domain, which is displayed by the $(\alpha3)_3(\beta4)_2$ stoichiometry but not by $(\alpha3)_2(\beta4)_3$. This specificity for a particular stoichiometry is remarkable and suggests that ribbon isoforms of α-conotoxins might have great potential in drug design. In this study, we investigated the binding mode and structure-activity relationships of ribbon AuIB using a combination of molecular modeling and electrophysiology recording to determine the features that underpin its selectivity. An alanine scan showed that positions 4 and 9 of ribbon AuIB are the main determinants of the interaction with $(\alpha3)_3(\beta4)_2$ nAChR. Our computational models indicate that the first loop of ribbon AuIB binds in the "aromatic box" of the acetylcholine orthosteric binding site, similar to that of globular AuIB. In contrast, the second loop and the termini of the ribbon isomer have different orientations and interactions in the binding sites to those of the globular isomer. The structure-activity relationships reported herein should be useful to design peptides displaying a ribbon α-conotoxin scaffold for inhibition of nAChR subtypes that have hitherto been difficult to selectively target.

Abbreviations

ACh, acetylcholine; AChBP, acetylcholine-binding protein; ECD, extracellular domain; gAuIB, globular AuIB; ICD, intracellular domain; nAChR, nicotinic acetylcholine receptor; rAuIB, ribbon AuIB; SAR, structure-activity relationship; TMD, transmembrane domain

Keywords: Conotoxin; Nicotinic acetylcholine receptor; Biological activity; Molecular modeling

Introduction

Nicotinic acetylcholine receptors (nAChRs) are pentameric ligand-gated cation-selective ion channels that belong to the Cys-loop family of receptors [1]. Neuronal nAChRs are homo- or heteropentamers of α2–α10 and β2–β4 subunits, and the different pentameric isoforms are differentially expressed in different parts of the brain [2,3]. Neuronal nAChR isoforms are involved in a range of diseases and conditions, including Alzheimer's disease, Parkinson's disease, schizophrenia, epilepsy, nicotine addiction, anxiety, depression and pain [3].

Heteropentameric nAChRs can assemble into different stoichiometries, with some displaying diverse pharmacological and biophysical properties [3]. For example, the α4β2 nAChR subtype, which is the most abundant nAChR subtype in the human brain, exists in two main stoichiometries: $(\alpha4)_2(\beta2)_3$ and $(\alpha4)_3(\beta2)_2$ [4]. These two stoichiometries have contrasting pharmacological properties: the $(\alpha4)_2(\beta2)_3$ has a long open lifetime and is insensitive to the agonist NS-9283, whereas the $(\alpha4)_3(\beta2)_2$ has a short open lifetime and is potentiated by NS-9283 [4]. Subunit stoichiometries of other nAChR subtypes such as the α3β4, α7β2 and α9α10 nAChR have also been reported [5–7]. Although the various subunit stoichiometries of these nAChR subtypes have disparate functions, the relationship between the different functions and pathophysiology states remains unknown, mostly because detecting nAChR subtype stoichiometries is challenging. In this study we established some groundwork on the structure-activity relationship (SAR) of the ribbon isoform of α-conotoxin AuIB (rAuIB) [8,9], which specifically inhibits one of the two major stoichiometries of the α3β4 nAChR [10].

Structurally, nAChRs are composed of three domains: an extracellular domain (ECD), a transmembrane domain (TMD), and an intracellular domain (ICD), as shown in Fig. 1 [1,11]. Acetylcholine (ACh) binds at the interface between two subunits in the ECD,

triggering the opening of the channel [1]. Each subunit in the ECD is composed of one α-helix, which lines the pore, and two β-sheets made of 10 β-strands (Fig. 1A and B). The ACh orthosteric binding site is located at the interface between two subunits in the ECD; the "principal" subunit, denoted (+), contacts the agonist with the A-, B- and C-loops, and the "complementary" subunit, denoted (−), contributes to the ACh binding site through the β-strands 2, 5 and 6 (Fig. 1B). Functional binding sites cannot be formed with β subunits as the principal subunit; therefore the number of functional binding sites displayed by heteropentameric nAChRs depend on their stoichiometries. As illustrated in Fig. 1C, the $(\alpha3)_2(\beta4)_3$ nAChR subtype has two α3(+)β4(−) functional binding sites, and the $(\alpha3)_3(\beta4)_2$ subtype has an additional functional binding site between two α3 subunits, i.e. α3(+)α3(−) [6]. Concatemeric assemblies of α3 and β4 subunits with the arrangements described in Figure 1C were reported to have similar pharmacological properties to subtypes assembled freely from subunits expressed in oocytes [12]. We note that in the current study we focused on engineered α3-containing nAChRs of these compositions but in native tissue the ganglionic nAChRs are more complex and could include accessory subunits of α3, α5, α6, β2 or β4 [13].

Conotoxins are a large family of disulfide-rich peptides isolated from the venom of marine cone snails [14,15]. Due to their potency and exquisite selectivity for ion channels and transporters of the nervous system, these peptides are considered as valuable pharmacological tools and drug leads [16]. The largest characterized pharmacological class of conotoxins are the α-conotoxins, which inhibit nAChRs and typically have 12–20 amino acid residues [14,16]. Because of their small size, α-conotoxins can readily be chemically synthesized, and their selectivity and potency against important nAChR subtypes make them interesting candidate drug leads [16–18]. Most α-conotoxins have the cysteine pattern CC-C-C, corresponding to the conotoxin cysteine Framework I. These conotoxins are further classified into *m*/*n* groups according to the length of the two loops, which are defined as the segments

between Cys II and Cys III (loop 1, *m* residues) and between Cys III and Cys IV (loop 2, *n* residues) [19,20]. The four Cys residues can theoretically form three disulfide connectivities, resulting in the globular isomer (Cys I-III, Cys II-IV), ribbon isomer (Cys I-IV, Cys II-III) or bead isomer (Cys I-II, Cys III-IV) (Fig. 1D). The globular isomer is typically displayed by wild-type α-conotoxins isolated from venoms, apart from one instance where the ribbon connectivity of an α-conotoxin was detected in the venom of *Conus imperialis* [21]. Some ribbon isomers are as active as or more potent than the globular isomer at inhibiting nAChRs, and consequently display altered pharmacological properties [8,22].

α-Conotoxin AuIB (Fig. 1D and E) belongs to the 4/6 class of conotoxins [9], and the globular form (gAuIB) inhibits the rat α3β4 nAChR with an IC_{50} of 1−3 μM [10]. rAuIB was the first ribbon isomer reported to have higher potency than the globular isomer, with rAuIB displaying a 10-fold improved inhibition of Ach-evoked current in rat parasympathetic neurons compared to gAuIB, with IC_{50}s of 0.1 nM and 1.2 nM, respectively [8]. However, another study reported that gAuIB was more potent than rAuIB at inhibiting rat α3β4 nAChR expressed in *Xenopus laevis* oocytes [23]. These apparently conflicting results were explained by a switch in the major stoichiometry of the α3β4 nAChR when expressed in mammalian cells compared to *X. laevis* oocytes [6]. AuIB isomers were shown to have differential sensitivity to the two stoichiometries of the α3β4 nAChR: gAuIB inhibited the $(\alpha3)_3(\beta4)_2$ nAChR (transfected at 10:1 ratio) and $(\alpha3)_2(\beta4)_3$ nAChR (1:10 ratio) with IC_{50}s of 1.1 μM and 3.0 μM, respectively; whereas rAuIB inhibited the $(\alpha3)_3(\beta4)_2$ nAChR with an IC_{50} of 0.86 μM and was inactive at the other stoichiometry [10]. Therefore, rAuIB only inhibited the stoichiometry displaying an α3(+)α3(−) binding site, indicating that it binds at the interface between two α3 subunits. Conotoxin rAuIB can therefore potentially be used to identify a single subtype and stoichiometry among all α3β4 subtypes expressed *in vivo*.

As the α3β4 nAChR subtype is involved in a range of drug addictions, (e.g. for morphine [24], methamphetamine [25] and nicotine [26–28]), and the β4 subunit is linked to anxiety behavior [29], these receptors are of considerable pharmaceutical interest. Thus, high-affinity molecular probes are required to tease apart the neurological functions of the two main α3β4 nAChR stoichiometries. Here, we investigated the SAR and binding mode of rAuIB on the rat α3β4 nAChR putatively expressed as $(\alpha3)_3(\beta4)_2$ stoichiometry from the injection of 10:1 α3:β4 RNA ratio. This is the first detailed SAR study of the binding mode of a ribbon α-conotoxin.

Materials and methods

2.1 Peptide synthesis and cleavage

A suite of 13 AuIB peptides (gAuIB, rAuIB, 10 Ala variants of rAuIB and [P7A]gAuIB) was synthesized using Fmoc solid phase peptide synthesis (SPPS) on a rink amide resin (Novabiochem®, Merck, Kenilworth, NJ, USA), with the side chains of Cys residues protected in pairs using orthogonal protective groups, which were then selectively removed in different oxidation solutions. For this purpose, we used the acid labile trityl (Trt) group to protect Cys II and Cys III, and the S-acetamidomethyl (Acm) group to protect Cys I and Cys IV for rAuIB and its mutants. Likewise for gAuIB, the Trt group was used to protect Cys II and Cys IV, and the Acm group was used to protect Cys I and Cys III. All crude linear peptides were cleaved and deprotected in a cleavage cocktail comprising 96% trifluoroacetic acid (TFA, Auspep, VIC, Australia), 2% H_2O and 2% triisopropylsilane (v/v) for 2 h. The crude peptides were purified by HPLC using a gradient of 0–50% buffer B (0.045% TFA in 90% acetonitrile [Merck]) over 50 min and monitoring at 214/280 nm. The same method was also used in subsequent purifications.

A two-step oxidative folding was used to form the disulfide bonds; the first disulfide bond was formed by adding peptides (80 mg crude peptide dissolved in 100 mL water) into an

equal volume of 20 mM potassium ferricyanide, 0.1 M Tris, pH 7.5 for 1 h. The reaction mixture was frozen and lyophilized overnight, and the second disulfide bond was formed by adding 50 mL of 0.1 M iodine solution for 1 h. All Fmoc-amino acids were from Chem-Impex International (Wood Dale, IL, USA). All organic reagents and solvents, unless stated otherwise, were purchased from Sigma-Aldrich (St Louis, MO, USA).

2.2 Nuclear magnetic resonance (NMR) spectroscopy

With a few exceptions, where crystallization has been possible [30], NMR is the preferred technique for conotoxin structural characterization. Two-dimensional total correlation spectroscopy (TOCSY) and nuclear Overhauser effect spectroscopy (NOESY) spectra of rAuIB, gAuIB and the variants were acquired using an Avance-600 MHz NMR spectrometer (Bruker) with mixing times of 80 ms and 200–300 ms, respectively. The α-proton (Hα) chemical shifts of synthetic peptides were assigned using CcpNmr analysis (version 2.4.1). Subsequently, the differences between the observed Hα chemical shifts and those of the corresponding residues in a random coil peptide [31], referred to as secondary Hα chemical shifts, were calculated to provide information on folding and secondary structure, as has been widely applied for other conotoxins [32].

2.3 In vitro cRNA synthesis

Plasmid constructs of rat α3 (pT7TS) and β4 (pNKS2) nAChR subunits were linearized with the XbaI restriction enzyme (NEB, Ipswich, MA, USA) for *in vitro* cRNA transcription using the T7/SP6 mMessage mMachine® transcription kits (AMBION, Forster City, CA, USA).

2.4 Oocyte preparation and microinjection

Stage V–VI oocytes were obtained from *X. laevis*, defolliculated with 1.5 mg/mL collagenase Type II (Worthington Biochemical Corp., Lakewood, NJ, USA) at room temperature (21–23 °C) for 1–2 h in OR-2 solution (82.5 mM NaCl, 2 mM KCl, 1 mM

$MgCl_2$ and 5 mM HEPES at pH 7.4). Oocytes were injected with 5 ng cRNA of rat α3β4 nAChR (α3:β4 = 10:1; concentration confirmed spectrophotometrically and by gel electrophoresis) using glass pipettes pulled from glass capillaries (3-000-203 GX, Drummond Scientific Co., Broomall, PA, USA). Oocytes were incubated at 18 °C in sterile ND96 solution (96 mM NaCl, 2 mM KCl, 1 mM $CaCl_2$, 1 mM $MgCl_2$ and 5 mM HEPES at pH 7.4), supplemented with 5% fetal bovine serum, 0.1 mg/mL gentamicin (Gibco, Grand Island, NY, USA) and 100 U/mL penicillin-streptomycin (Gibco, Grand Island, NY, USA).

2.5 Oocyte two-electrode voltage clamp recording and data analysis

Electrophysiological recordings were carried out 2–5 days post cRNA microinjection. Two-electrode voltage clamp recordings were performed at room temperature using a GeneClamp 500B amplifier and pClamp9 software interface (Molecular Devices, Sunnyvale, CA, USA) at a holding potential of −80 mV. Voltage-recording and current-injecting electrodes were pulled from GC150T-7.5 borosilicate glass (Harvard Apparatus, Holliston, MA, USA) and filled with 3 M KCl, giving resistances of 0.3–1 MΩ. Oocytes were perfused with ND96 solution using a continuous Legato 270 push/pull syringe pump perfusion system (KD Scientific, Holliston, MA, USA) at a rate of 2 mL/min.

Initially, oocytes were briefly washed with ND96 solution followed by three applications of 50 μM ACh for rat α3β4 nAChR (α3:β4 = 10:1) [10]. Washout with bath solution was done for 3 min between ACh applications. Oocytes were incubated with peptides for 5 min with the perfusion system turned off, followed by co-application of ACh and peptide with flowing bath solution. All peptide solutions were prepared in ND96 solution containing 0.1% bovine serum albumin. Peak current amplitudes before (ACh alone) and after (ACh + peptide) peptide incubation were measured using AxoGraph X software (Axograph Scientific, Berkeley, CA, USA), where the ratio of ACh + peptide-evoked current amplitude

to ACh alone-evoked current amplitude was used to assess the activity of the peptides at the rat α3β4 nAChR.

All electrophysiological data were pooled ($n \geq 3$) and represent means ± standard error of the mean. Data sets were compared using an unpaired Student's t-test (GraphPad Software, La Jolla, CA, USA). Differences were regarded statistically significant when $p < 0.05$. The IC_{50} was determined from concentration-response curve fitted to a non-linear regression function and reported with error of the fit.

2.6 Molecular modeling

Molecular models of the interaction between AuIB and the ECD of rat α3β4 nAChR were built by homology with Modeller9v18 [33] using the following crystal structures as templates: (1) the complex between *Aplysia californica* acetylcholine-binding protein (AChBP) and conotoxin PnIA variant (PDB: 2BR8), and (2) the human α4β2 nAChR (PDB: 5KXI). The complex between rAuIB and the ECD of $(\alpha3)_3(\beta4)_2$ nAChR was modelled by assuming an interaction in the α3(+)α3(−) orthosteric binding site whereas the complex between gAuIB and the ECD of $(\alpha3)_2(\beta4)_3$ nAChR was built by assuming an interaction in the α3(+)β4(−) orthosteric binding site. Similar to most other α-conotoxins rAuIB is a competitive inhibitor of the α3β4 nAChR, suggesting that it binds in the orthosteric binding site [10]. In contrast, α-conotoxin gAuIB inhibits non-competitively the α3β4 nAChR [10] but it was shown to nevertheless bind to the orthosteric binding site [34]. This latter study unequivocally identified that gAuIB binds at the α3(+)β4(−) interface using electrophysiological recording of nAChRs expressing β4 subunit mutants. As an explanation to the non-competitive nature of the inhibition, gAuIB was proposed to stabilize the desensitized state of α3β4 nAChR [34]. It was previously demonstrated using single channel recording that another antagonist, DHβE, stabilized the desensitized state of an nAChR [35], despite binding in the orthosteric binding site [36].

The molecular models were refined by a 50 ns molecular dynamics simulation in explicit water using the GROMACS 5.1.4 package [37] and the Amber99SB-ILDN protein force field [38], as described previously [39,40]. Briefly, the systems were gradually heated from 50 to 300 K at constant volume and then simulated with constant pressure while gradually removing the restraints imposed on the protein and peptide atoms. All bonds involving hydrogen atoms were constrained with the LINCS algorithm, allowing the use of a 2 fs time step. The particle-mesh Ewald method was used to compute long-range electrostatic interactions. The models of complexes involving two rAuIB mutants, [S4A]rAuIB and [F9A]rAuIB, were initially generated by substituting residue side chains using Modeller9v18 and then carrying out molecular dynamics simulations as described above. The backbone root-mean-square deviation from the starting conformation was stable over the last 20 ns of the simulations and this period was used for analysis. The solvent accessible surface area was calculated using the GROMACS package with a probe radius of 1.4 Å. Additional 200 ns molecular dynamics simulations were also carried out using similar set-up for rAuIB and [P7A]rAuIB in the absence of the receptor. Secondary structure analyses of these simulations were computed using the DSSP program [41] and the GROMACS package.

Results

3.1 Peptide synthesis and oxidative folding

We designed a suite of mutants in which all non-Cys residues of rAuIB were separately substituted by Ala to identify the positions that are important for inhibition of the α3β4 nAChR (Table 1). All the Ala mutants of rAuIB as well as rAuIB, gAuIB and [P7A]gAuIB were successfully synthesized with orthogonal protection of the cysteine side chains to orient the folding toward a unique disulfide isomer.

3.2 [P7A]rAuIB has more similar secondary Hα chemical shifts to gAuIB than rAuIB

Secondary Hα chemical shifts analysis, which is useful for deducing secondary structure elements, was conducted for gAuIB, rAuIB and all mutants (Fig. 2). The Hα secondary chemical shifts of rAuIB synthesized in this study were in agreement with previously reported values [8], indicating that the fold of rAuIB is the same as in previous studies. Apart from some local changes in chemical shift at the substitution site, all mutants displayed a similar pattern of shifts to the parent peptide except [P7A]rAuIB (Fig. 2C). Interestingly, residues from Pro6 to Phe9 of [P7A]rAuIB had negative secondary Hα chemical shifts (Fig. 2C), indicating that this segment adopts an α-helical structure, a motif that exists in the globular isomer but not in the ribbon isomer. The P7A substitution therefore seems to have improved the definition of the structure of rAuIB, with the parent peptide being devoid of stable regular secondary structure. The retention time and secondary Hα chemical shifts between [P7A]rAuIB and [P7A]gAuIB were different, excluding the possibility that [P7A]rAuIB converted into [P7A]gAuIB during the folding process (Fig. 2D). To further substantiate this difference of conformation, we carried out two 200 ns molecular dynamics simulations: one simulation starting from the NMR solution structure of rAuIB, and the second from a model of the P7A variant, which was created by simple side chain swaps in the NMR structure of rAuIB. Consistent with the NMR measurements, the simulation of [P7A]rAuIB suggested the existence of a stable α-helix from Pro6 to Phe9 (Fig. 2E). Interestingly, the P7A variant was more rigid than the parent peptide, as measured using the root-mean-square fluctuation (Fig. 2F).

3.3 Several rAuIB analogues have decreased potency at rat α3β4 nAChR

All peptides were tested for inhibition of the rat α3β4 nAChR subtype heterologously expressed in *X. laevis* oocytes. In the first round of electrophysiological experiments, all rAuIB Ala mutants were tested at 1 μM (corresponding to the reported IC_{50} of rAuIB [10])

and gAuIB was tested at 3 μM, resulting in 30–40% inhibition of ACh-evoked currents of rat α3β4 (α3:β4 = 10:1) nAChR (Fig. 3A). The rAuIB Ala mutants exhibited comparable activity to the parent peptide except for [S4A] and [F9A]rAuIB, which caused 25% and 20% inhibition, respectively (Fig. 3A). Comparison of the rat α3β4 nAChR inhibition by [S4A] and [F9A]rAuIB indicates that the difference was not statistically significant. In the second round, all peptides were tested at 100 μM, inhibiting 35–55% of ACh-evoked currents of rat α3β4 (α3:β4 = 10:1) nAChR (Fig. 3A). Mutation at S4, P6, F9, T11, N12 and D14 caused a decrease in activity, *ca.* 40% inhibition, whereas other peptides had higher activity, with 45–55% inhibition (Fig. 3B and C). The efficacy (maximum inhibition of ACh-evoked currents) of rAuIB was ~55%, which is ~15% lower than reported previously [10]. This difference may arise from variations in the relative levels of expression of α3 and β4 subunits in different batches of oocytes.

In summary, none of the single position variants displayed a dramatic loss of activity compared to the parent peptide. The Ala substitution of six positions in rAuIB led to a decreased activity at high concentration, but only two substitutions, S4A and F9A, significantly impacted activity at a concentration similar to the IC_{50} of rAuIB, suggesting they are more important for antagonizing the activity of rat α3β4 nAChR. To better quantify the loss of activity, we calculated the IC_{50} of [S4A]rAuIB at the α3β4 nAChR (α3:β4 = 10:1) to be 442 ± 99 nM (Fig. 3D); the IC_{50} of rAuIB was previously reported to be 860 nM at the same receptor stoichiometry [10]. Considering the variability between different electrophysiological set-ups, we consider that inhibition by rAuIB and [S4A] rAuIB are of the same order of magnitude, i.e., the S4A substitution caused a less than 10-fold drop decrease in inhibition.

3.4 rAuIB adopts a binding mode similar to that of globular α-conotoxins

Since the functional data indicated that rAuIB inhibits the α3(+)α3(−) interface of the $(\alpha3)_3(\beta4)_2$ nAChR [10] we built molecular models of the interaction between the α3(+)α3(−) binding site and rAuIB. This model was refined using molecular dynamics simulations and used to propose explanations for the SAR data. A molecular model of the interaction between gAuIB and the α3(+)β4(−) binding site was built similarly to that of rAuIB for comparison purposes. The molecular interactions between the peptides and the receptors were monitored over the last 20 ns of each 50 ns simulation. This period of 20 ns, during which the system reached equilibrium, is referred to as the "simulation time".

3.4.1 Binding mode of gAuIB at the rat α3β4 nAChR

The G1A, P6A and F9A mutants of gAuIB are reported to display decreased inhibitory activity at rat α3β4 nAChR compared to gAuIB [34]. The molecular model of the complex between gAuIB and the α3(+)β4(−) binding site (Fig. 4A), which is very similar to a reported molecular model of the same system [34], can be used to suggest rational explanations to the consequence of these substitutions. The positively charged N-terminus (Gly1) is in the proximity of the negatively charged side chain oxygen atoms of D168 and D169 in the simulation, with an average distance of 3.9 Å and 2.8 Å. A stable salt bridge was established between D169 and the N-terminus during the simulation time and a similar interaction was transiently formed between D169 and the N-terminus. Therefore, a substitution of this first residue of the toxin by Ala could change the peptide backbone conformation and prevent the establishment of these salt bridges.

Pro6 is a highly conserved residue among α-conotoxins because it anchors the conotoxins into an aromatic pocket on the nAChR that is important for the interaction between nAChR and agonists [42]. It is therefore not surprising that the substitution of Pro6 by Ala caused a decrease in activity. The side chain of Phe9 is embedded in a hydrophobic

pocket formed by K57, E59, Q117 and L119 of the β4 subunit, and the backbone oxygen of Phe9 formed a hydrogen bond with the receptor Q117 during 85% of the simulation time. The substitution of the bulky Phe9 by an Ala, which has a smaller side chain, would cause a change in shape complementarity at the interface, possibly resulting in a reorientation of the peptide in the binding pocket (similar to [F9A]rAuIB described below).

3.4.2 Binding mode of rAuIB at the rat α3β4 nAChR

Our molecular models suggest that the conformation adopted by rAuIB when bound to the rat α3β4 nAChR is similar to that of gAuIB except for the N- and C- termini (Fig. 4B). The interactions established by the first loop of AuIB are similar for the two isomers, and this loop sits deeply in the orthosteric binding site of the α3β4 nAChR. The first disulfide bond (i.e., Cys I-Cys III for gAuIB and Cys I-Cys IV for rAuIB) packs similarly against the vicinal disulfide bond of the C-loop, and this interaction is a conserved feature in the crystal structures of α-conotoxins/AChBP. Because of this interaction, the different disulfide connectivities of the two isomers resulted in different peptide conformation and disparate location of their N- and C- termini within the nAChR binding site. The charged N-terminus, (Gly1) interacts with the acidic residues of the F-loop of α3β4 nAChR in the gAuIB model (Fig. 4A) but not in the model of rAuIB (Fig. 4B). The location of the amidated C-terminus in the nAChR binding site is also different between the two isomers; this difference results from the different conformation of the second loop.

We have shown the side chains of Ser4 and Phe9 in rAuIB are the most important for activity at the rat α3β4 nAChR. As shown in Fig. 4B, Ser4 of rAuIB establishes a stable side chain-side chain hydrogen bond with D169 (98% of the simulation time). Additionally, Ser4 forms transient hydrogen bonds with S36 and N166 (40% of the simulation time). Phe9 of rAuIB interacts with the α3(−) subunit: it forms a hydrogen bond with K57 through its backbone oxygen during 93% of the simulation and its side chain contacts the residues E34,

S36, W55, K57 and I119. The distance between the heavy atoms of Phe9 and of the aforementioned residues of the α3(−) subunit were below 5.0 Å, the distance considered to define a contact.

Positions 11, 12 and 14 of rAuIB caused a small drop of inhibition when mutated to Ala. These three residues are located at the interface with the receptor in the binding model but their side chains are also solvated, suggesting that their contribution to the electrostatic component of the binding energy is at best weak. Indeed, their involvement was only detected experimentally at the highest concentration (100 μM). By contrast, the impact of the substitutions S4A and F9A were detected at the lower concentration of 1 μM. We further studied the impact of these two substitutions on the binding mode by carrying out further molecular dynamics simulations.

3.4.3 Binding mode of [S4A]rAuIB at the rat α3β4 nAChR

The binding mode resulting from the 50 ns molecular dynamics simulation of [S4A]rAuIB displayed subtle variations from that of the parent peptide, with differences mainly located in the proximity of the modified position 4 (Fig. 4C). Besides position 4, all positions at the interface with the β4 subunit, such as Phe9, established similar molecular interactions in the S4A mutated model. The simulation suggests that the loss of the hydrogen bond between Ser4 and D169 is compensated by the establishment of a hydrogen bond between the side chain of α3(−) K168 and the backbone oxygen of the toxin Cys2, which was stable for 89% of the simulation time. The conformation of the side chain of K168 of the receptor seems to be also stabilized by electrostatic interactions with the D169 side chain. This electrostatic interaction was not possible in the rAuIB model because D169 was engaged in a hydrogen bond with Ser4 and consequently maintained away from K168 (Fig. 4B and C). The transient hydrogen bonds between Ser4 and α3(−) S36/N166 established in the model of rAuIB were not compensated in the mutated model of [S4A]rAuIB. Therefore, we suggest

that [S4A]rAuIB displays overall fewer hydrogen bonds with the receptor than the parent peptide. Based on electrophysiological measurements, we proposed that the decrease in activity was lower than 10-fold, corresponding to a loss of less than 1.4 kcal/mol. This energy is typical of a weak hydrogen bond interaction, which is consistent with the 40% occurrence of the hydrogen bonds between Ser4 and S36/N166 during the molecular dynamics simulations.

3.4.4 Binding mode of [F9A]rAuIB at the rat α3β4 nAChR

According to the molecular model of rAuIB bound to the α3(+)α3(−) binding site, Phe9 is buried at the interface with the receptor. Its substitution by Ala creates a gap between the α3(−) subunit and the peptide in the initial step of the simulation. During this simulation, the peptide reoriented slightly in the binding site, resulting in several changes of pairwise interactions and a slight outward reorientation of the C-loop (Fig. 4D). Globally, the F9A variant had fewer contacts with the receptor than the parent peptide, as evidenced by a decrease in buried surface area from 1646 $Å^2$ to 1452 $Å^2$. As a result of the slight shift in orientation, the backbone oxygen of Ala9 only forms a transient hydrogen bond (42% of the simulation time) with the side chain of K57, whereas this interaction was present during 93% of the simulation time for the parent peptide. Similarly, the hydrogen bond between Ser4 (rAuIB) and D169 (α3 subunit) of the receptor was only observed during 75% of the simulation time compared to 98% for the parent peptide. We therefore propose that the F9A substitution caused a slight shift of the binding mode, resulting in fewer contacts and hydrogen bonds at the interface.

Discussion

The surprising discovery that the ribbon isomer of an α-conotoxin displays higher potency than the corresponding globular isomer [8] contrasts with the previously held assumption that native (globular) disulfide isomers have optimal activity. We carried out a

complete Ala scan of rAuIB, discovering the side chains of two positions, Ser4 and Phe9, were the most important for activity against the rat α3β4 nAChR. We have rationalized these data by proposing a binding mode between rAuIB and α3β4 nAChR. Molecular dynamics simulation suggested that rAuIB adopts a well-defined conformation when bound to its molecular target and that the binding mode is highly stable. A number of other SAR studies have been conducted on globular α-conotoxins [14], and we compared our results to these studies to further evaluate the molecular model of rAuIB binding mode.

Position 1 was identified to be important for gAuIB activity at the α3β4 nAChR [34] but this was not the case for rAuIB (this study), paralleling the contrasting role of this position observed in several other studies on α-conotoxins. As for rAuIB, the G1A substitution had no impact on the inhibition of α7 nAChR by α-conotoxin ImI [43], and a minor impact on the affinity of α-conotoxin MII for the α3β2 nAChR (< 5-fold difference) [44]. A molecular model of the interaction between ImI and the α7 nAChR indeed suggested that ImI Gly1 does not interact with the receptor [40], similar to our model of the rAuIB/α3β4 nAChR complex. In contrast, the G1A mutation of α-conotoxin TxID resulted in a ~20-fold decreased activity at the α3β4 nAChR [45], and the same substitution caused a significant decrease in activity for α-conotoxin gAuIB at the α3β4 nAChR [34]. The molecular models of the corresponding complexes suggested that the N-terminus of these peptides potentially forms a salt bridge with negatively charged residues located in the F-loop of the receptor [34,45], as in our model of the gAuIB/α3β4 nAChR complex.

The S4A substitution impacted the activity of rAuIB at the α3β4 nAChR, but it was reported not to affect that of gAuIB [34]. As for gAuIB, this substitution had no effect on the activity or affinity of α-conotoxin RgIA at α9α10 [46], ImI at α7 [43,47], PeIA at α3β2 and α6/α3β2β3 [48], BuIA at α6/α3β2β3 [49] and TxID at α3β4 nAChRs [45]. Only a small decrease of inhibition of five- to eight-fold was reported after a substitution equivalent to S4A

in GID* (S7A for GID*) and MII at the α4β2 and α3β2 nAChRs, respectively [44,50,51]. TxID Ser4 was suggested to have no interaction with the receptor using molecular modeling, explaining that its substitution to Ala was innocuous [45]. In contrast, a molecular model of the complexes involving GID* and the α4β2 nAChR suggested that the Ser side chain potentially forms a hydrogen bond with an Asp residue in the F-loop of the receptor [52], similar to our model of the rAuIB/α3β4 nAChR complex.

Pro6 is highly conserved among all α-conotoxins and typically interacts with the aromatic box, which is a conserved ACh interaction site in the nAChR and AChBP orthosteric binding sites [53–55]. Pro6 is also important for stabilizing the structure of globular α-conotoxins: replacing this Pro with Ala typically results in a change of conformation linked to a decrease or loss of activity. For example, the P6A substitution of α-conotoxin PeIA caused a 20-fold decrease of inhibition of the α6/α3β2β3 nAChR compared to the parent peptide [48]. The P6A substitution of α-conotoxins ImI and MI resulted in a 50–70 fold decrease in affinity for the α7 and muscle type nAChRs, respectively [43,47,56], whereas this substitution caused a >700-fold decrease in activity for α-conotoxin MII at the α3β2 nAChR [44,50]. The same substitution resulted in a loss of helical content for globular Vc1.1 and a marked decrease in inhibitory activity of α-conotoxin Vc1.1 [57]. Similarly, the P6A substitution of gAuIB resulted in a decrease in secondary structure content as well as a complete loss of inhibitory activity [34]. In contrast, [P6A]rAuIB showed only a small decrease in activity compared to the parent peptide. Our molecular models suggest that Pro6 of rAuIB and gAuIB should make similar interactions with the receptor and we propose that the different impact that P6A substitution had on the activity of the two peptides arises from its differential effect on the peptide structures. Indeed, P6A substitution destabilizes the small α-helical motif required for the activity of gAuIB. In contrast, as rAuIB already lacks regular secondary structure, P6A does not further impact its propensity to adopt the α-helical content required for binding to the

receptor. The substantial decrease in inhibitory activity of gAuIB resulting from P6A substitution appears therefore to result primarily from the change of conformation of the peptide rather than decreased interactions of the position 6 side chain at the interface.

The only rAuIB variant that displayed different Hα secondary chemical shifts from the parent peptide was [P7A]rAuIB, indicating that this variant adopts a different fold in solution. NMR spectroscopy data suggest that [P7A]rAuIB adopts a helical structure, whereas rAuIB lacked regular secondary structure and was globally less structured. A possible explanation for this change of conformation is that Ala residues promote the formation of α-helices, whereas Pro residues typically destabilize regular secondary structure elements. BuIA is the only other α-conotoxin that has a similar cysteine scaffold to AuIB and had its ribbon isomer studied by NMR spectroscopy [58]. As for ribbon AuIB, ribbon BuIA displays Pro residues at positions 6 and 7. The ribbon isomer of BuIA also has a more flexible backbone than the globular isomer and does not form the α-helix that is a conserved feature of α-conotoxin globular isomers. It would be interesting to study the influence of the P7A substitution on the structure of ribbon BuIA because this substitution could increase the helical content similarly to rAuIB. In our molecular models, rAuIB interacts with the receptor using a conformation that is stabilized by the P7A substitution, suggesting that the binding energy of the variant would benefit from a more favourable entropy term than the parent peptide. Nevertheless, the activity of the mutant was not experimentally different from the parent peptide, which could be interpreted by the loss of a number of contacts between the Pro side chain and the receptor.

The substitution of position 9 with Ala caused a decrease in affinity for both gAuIB [34] and rAuIB (this work). Position 9 of globular α-conotoxins is buried at the interface with the complementary subunit and has been identified as important for modulating the activity of a range of globular α-conotoxins [34,45,46,49,51,57]. For example, Ala mutation at this position caused a 50-fold decrease in activity of α-conotoxin GI at the muscle type nAChR

[59], a 20–30 fold decrease in affinity of α-conotoxin MII at α3β2 nAChR [44,50], and a >17-fold decrease in activity of α-conotoxin GID* at α4β2 nAChR [51]. In addition, the R9A substitution resulted in a 1500-fold decrease in activity of RgIA at α9α10 nAChR [46]. Substitution of position 9 can also enhance activity, with the [S9A]PeIA displaying three-fold lower IC_{50} than the parent peptide at the α3β2 nAChR [48] and the [N9W]Vc1.1 and [N9A]Vc1.1 increasing activity by 20- and 30-fold at the human α9α10 nAChR compared to Vc1.1, respectively [39,57]. Several molecular models have been built to explain the ability of α-conotoxin position 9 to modulate nAChR inhibition, which suggest this residue interacts with various positions of the complementary subunit depending on the conotoxin and nAChR subtype [39,52,60]. In the proposed binding mode of rAuIB, Phe9 mainly interacts with β4 K57, whereas GID* Arg12 was proposed to interact with β2 position 59 [52], [N9W]Vc1.1 Trp9 with α10 W118 [39] and RgIA Arg9 with α10 W81 [60].

In summary, we have identified a number of positions crucial for the activity of the ribbon isomer of AuIB that are also important for the activity of gAuIB and/or other globular α-conotoxins, indicating rAuIB has a globally similar binding mode to the globular isomers of α-conotoxins. According to our models, the main difference between the ribbon and globular AuIB at the interface with α3β4 nAChR is at their N- and C- termini. Changing the disulfide connectivity of α-conotoxins from a globular to ribbon isomer therefore does not introduce a dramatic change of binding mode at the interface with the receptor but it does create some different interactions that can have a substantial impact on the selectivity, as is the case for AuIB. Ribbon isomers should therefore be more systematically considered in the design of molecular probes and specific inhibitors of nAChR subtypes based on α-conotoxins.

Acknowledgements

This work was funded by the Australian Research Council (DP150103990). DJC is an ARC Australian Laureate Fellow (FL150100146). We thank Olivier Cheneval (Institute for Molecular Bioscience, The University of Queensland) for synthesising peptides.

Conflict of interest: The authors declare that they have no conflict of interest.

References

[1] M. Cecchini, J.-P. Changeux, The nicotinic acetylcholine receptor and its prokaryotic homologues: Structure, conformational transitions & allosteric modulation, Neuropharmacology. 96 (2015) 137–149. doi:10.1016/j.neuropharm.2014.12.006.

[2] E.X. Albuquerque, E.F.R. Pereira, M. Alkondon, S.W. Rogers, Mammalian nicotinic acetylcholine receptors: from structure to function, Physiol. Rev. 89 (2009) 73–120. doi:10.1152/physrev.00015.2008.

[3] M. Zoli, F. Pistillo, C. Gotti, Diversity of native nicotinic receptor subtypes in mammalian brain, Neuropharmacology. 96 (2015) 302–311. doi:10.1016/j.neuropharm.2014.11.003.

[4] S. Mazzaferro, I. Bermudez, S.M. Sine, α4β2 Nicotinic acetylcholine receptors: relationships between subunit stoichiometry and function at the single channel level, J. Biol. Chem. 292 (2017) 2729–2740. doi:10.1074/jbc.M116.764183.

[5] D.C. Indurthi, E. Pera, H.-L. Kim, C. Chu, M.D. McLeod, J.M. McIntosh, N.L. Absalom, M. Chebib, Presence of multiple binding sites on α9α10 nAChR receptors alludes to stoichiometric-dependent action of the α-conotoxin, Vc1.1, Biochem. Pharmacol. 89 (2014) 131–140. doi:10.1016/j.bcp.2014.02.002.

[6] P. Krashia, M. Moroni, S. Broadbent, G. Hofmann, S. Kracun, M. Beato, P.J. Groot-Kormelink, L.G. Sivilotti, Human α3β4 neuronal nicotinic receptors show different stoichiometry if they are expressed in Xenopus oocytes or mammalian HEK293 cells, PLoS One. 5 (2010) e13611. doi:10.1371/journal.pone.0013611.

[7] T.A. Murray, D. Bertrand, R.L. Papke, A.A. George, R. Pantoja, R. Srinivasan, Q. Liu, J. Wu, P. Whiteaker, H.A. Lester, R.J. Lukas, α7β2 nicotinic acetylcholine receptors assemble, function, and are activated primarily via their α7-α7 interfaces, Mol. Pharmacol. 81 (2012) 175–188. doi:10.1124/mol.111.074088.

[8] J.L. Dutton, P.S. Bansal, R.C. Hogg, D.J. Adams, P.F. Alewood, D.J. Craik, A new level of conotoxin diversity, a non-native disulfide bond connectivity in α-conotoxin AuIB reduces structural definition but increases biological activity, J. Biol. Chem. 277 (2002) 48849–57. doi:10.1074/jbc.M208842200.

[9] S. Luo, J.M. Kulak, G.E. Cartier, R.B. Jacobsen, D. Yoshikami, B.M. Olivera, J.M. McIntosh, α-conotoxin AuIB selectively blocks α3β4 nicotinic acetylcholine receptors and nicotine-evoked norepinephrine release, J. Neurosci. 18 (1998) 8571–8579. doi:10.1523/JNEUROSCI.18-21-08571.1998.

[10] A.A. Grishin, C.-I.A. Wang, M. Muttenthaler, P.F. Alewood, R.J. Lewis, D.J. Adams, α-conotoxin AuIB isomers exhibit distinct inhibitory mechanisms and differential sensitivity to stoichiometry of α3β4 nicotinic acetylcholine receptors, J. Biol. Chem. 285 (2010) 22254–22263. doi:10.1074/jbc.M110.111880.

[11] C.L. Morales-Perez, C.M. Noviello, R.E. Hibbs, X-ray structure of the human α4β2 nicotinic receptor, Nature. 538 (2016) 411–415. doi:10.1038/nature19785.

[12] A.A. George, L.M. Lucero, M.I. Damaj, R.J. Lukas, X. Chen, P. Whiteaker, Function of human α3β4α5 nicotinic acetylcholine receptors is reduced by the α5(D398N) variant, J. Biol. Chem. 287 (2012) 25151–25162. doi:10.1074/jbc.M112.379339.

[13] H. Cuny, R. Yu, H.-S. Tae, S.N. Kompella, D.J. Adams, α-Conotoxins active at α3-containing nicotinic acetylcholine receptors and their molecular determinants for selective inhibition, Br. J. Pharmacol. 175 (2018) 1855–1868. doi:10.1111/bph.13852.

[14] K.B. Akondi, M. Muttenthaler, S. Dutertre, Q. Kaas, D.J. Craik, R.J. Lewis, P.F. Alewood, Discovery, synthesis, and structure-activity relationships of conotoxins, Chem. Rev. 114 (2014) 5815–5847. doi:10.1021/cr400401e.

[15] Q. Kaas, R. Yu, A.-H. Jin, S. Dutertre, D.J. Craik, ConoServer: updated content, knowledge, and discovery tools in the conopeptide database, Nucleic Acids Res. 40 (2012) D325-330. doi:10.1093/nar/gkr886.

[16] H. Terlau, B.M. Olivera, Conus venoms: a rich source of novel ion channel-targeted peptides, Physiol. Rev. 84 (2004) 41–68. doi:10.1152/physrev.00020.2003.

[17] R. Halai, D.J. Craik, Conotoxins: natural product drug leads, Nat. Prod. Rep. 26 (2009) 526–536. doi:10.1039/B819311H.

[18] E.K.M. Lebbe, S. Peigneur, I. Wijesekara, J. Tytgat, Conotoxins targeting nicotinic acetylcholine receptors: an overview, Mar. Drugs. 12 (2014) 2970–3004. doi:10.3390/md12052970.

[19] L. Azam, J.M. McIntosh, Alpha-conotoxins as pharmacological probes of nicotinic acetylcholine receptors, Acta Pharmacol. Sin. 30 (2009) 771–783. doi:10.1038/aps.2009.47.

[20] R.W. Janes, α-Conotoxins as selective probes for nicotinic acetylcholine receptor subclasses, Curr. Opin. Pharmacol. 5 (2005) 280–292. doi:10.1016/j.coph.2005.01.013.

[21] H. Safavi-Hemami, D.G. Gorasia, A.M. Steiner, N.A. Williamson, J.A. Karas, J. Gajewiak, B.M. Olivera, G. Bulaj, A.W. Purcell, Modulation of conotoxin structure and function is achieved through a multienzyme complex in the venom glands of cone snails, J. Biol. Chem. (2012). doi:10.1074/jbc.M112.366781.

[22] B.B. Carstens, G. Berecki, J.T. Daniel, H.S. Lee, K.A.V. Jackson, H.-S. Tae, M. Sadeghi, J. Castro, T. O'Donnell, A. Deiteren, S.M. Brierley, D.J. Craik, D.J. Adams, R.J. Clark, Structure-activity studies of cysteine-rich α-conotoxins that inhibit high-voltage-activated calcium channels via GABA(B) receptor activation reveal a minimal functional motif, Angew. Chem. Int. Ed Engl. 55 (2016) 4692–4696. doi:10.1002/anie.201600297.

[23] A. Nicke, M. Samochocki, M.L. Loughnan, P.S. Bansal, A. Maelicke, R.J. Lewis, α-Conotoxins EpI and AuIB switch subtype selectivity and activity in native versus recombinant nicotinic acetylcholine receptors, FEBS Lett. 554 (2003) 219–223. doi:10.1016/S0014-5793(03)01161-X.

[24] O.D. Taraschenko, J.M. Shulan, I.M. Maisonneuve, S.D. Glick, 18-MC acts in the medial habenula and interpeduncular nucleus to attenuate dopamine sensitization to morphine in the nucleus accumbens, Synapse. 61 (2007) 547–560. doi:10.1002/syn.20396.

[25] S.D. Glick, I.M. Maisonneuve, B.A. Kitchen, M.W. Fleck, Antagonism of α3β4 nicotinic receptors as a strategy to reduce opioid and stimulant self-administration, Eur. J. Pharmacol. 438 (2002) 99–105. doi:10.1016/S0014-2999(02)01284-0.

[26] W. Berrettini, X. Yuan, F. Tozzi, K. Song, C. Francks, H. Chilcoat, D. Waterworth, P. Muglia, V. Mooser, α5/α3 nicotinic receptor subunit alleles increase risk for heavy smoking, Mol. Psychiatry. 13 (2008) 368–373. doi:10.1038/sj.mp.4002154.

[27] S.D. Glick, I.M. Maisonneuve, B.A. Kitchen, Modulation of nicotine self-administration in rats by combination therapy with agents blocking α3β4 nicotinic receptors, Eur. J. Pharmacol. 448 (2002) 185–191. doi:10.1016/S0014-2999(02)01944-1.

[28] I.M. Maisonneuve, S.D. Glick, Anti-addictive actions of an iboga alkaloid congener: a novel mechanism for a novel treatment, Pharmacol. Biochem. Behav. 75 (2003) 607–618. doi:10.1016/S0091-3057(03)00119-9.

[29] R. Salas, F. Pieri, B. Fung, J.A. Dani, M. De Biasi, Altered anxiety-related responses in mutant mice lacking the β4 subunit of the nicotinic receptor, J. Neurosci. 23 (2003) 6255–6263. doi:10.1523/JNEUROSCI.23-15-06255.2003.

[30] S.H. Hu, J. Gehrmann, P.F. Alewood, D.J. Craik, J.L. Martin, Crystal structure at 1.1 A resolution of α-conotoxin PnIB: comparison with α-conotoxins PnIA and GI, Biochemistry. 36 (1997) 11323–11330. doi:10.1021/bi9713052.

[31] D.S. Wishart, B.D. Sykes, The 13C Chemical-Shift Index: A simple method for the identification of protein secondary structure using 13C chemical-shift data, J Biomol. NMR. 4 (1994) 171–180.

[32] K.J. Nielsen, L. Thomas, R.J. Lewis, P.F. Alewood, D.J. Craik, A consensus structure for ω-conotoxins with different selectivities for voltage-sensitive calcium channel subtypes: Comparison of MVIIA, SVIB and SNX-202, J. Mol. Biol. 263 (1996) 297–310. doi:10.1006/jmbi.1996.0576.

[33] A. Sali, T.L. Blundell, Comparative protein modelling by satisfaction of spatial restraints, J. Mol. Biol. 234 (1993) 779–815. doi:10.1006/jmbi.1993.1626.

[34] A.A. Grishin, H. Cuny, A. Hung, R.J. Clark, A. Brust, K. Akondi, P.F. Alewood, D.J. Craik, D.J. Adams, Identifying key amino acid residues that affect α-conotoxin AuIB inhibition of α3β4 nicotinic acetylcholine receptors, J. Biol. Chem. 288 (2013) 34428–34442. doi:10.1074/jbc.M113.512582.

[35] D. Bertrand, A. Devillers-Thiéry, F. Revah, J.L. Galzi, N. Hussy, C. Mulle, S. Bertrand, M. Ballivet, J.P. Changeux, Unconventional pharmacology of a neuronal nicotinic receptor mutated in the channel domain, Proc. Natl. Acad. Sci. U. S. A. 89 (1992) 1261–1265.

[36] A. Shahsavar, J.S. Kastrup, E.Ø. Nielsen, J.L. Kristensen, M. Gajhede, T. Balle, Crystal Structure of Lymnaea stagnalis AChBP Complexed with the Potent nAChR Antagonist DHβE Suggests a Unique Mode of Antagonism, PLOS ONE. 7 (2012) e40757. doi:10.1371/journal.pone.0040757.

[37] M.J. Abraham, T. Murtola, R. Schulz, S. Páll, J.C. Smith, B. Hess, E. Lindahl, GROMACS: High performance molecular simulations through multi-level parallelism from laptops to supercomputers, SoftwareX. 1–2 (2015) 19–25. doi:10.1016/j.softx.2015.06.001.

[38] K. Lindorff-Larsen, S. Piana, K. Palmo, P. Maragakis, J.L. Klepeis, R.O. Dror, D.E. Shaw, Improved side-chain torsion potentials for the Amber ff99SB protein force field, Proteins. 78 (2010) 1950–1958. doi:10.1002/prot.22711.

[39] R. Yu, S.N. Kompella, D.J. Adams, D.J. Craik, Q. Kaas, Determination of the α-conotoxin Vc1.1 binding site on the α9α10 nicotinic acetylcholine receptor, J. Med. Chem. 56 (2013) 3557–3567. doi:10.1021/jm400041h.

[40] R. Yu, D.J. Craik, Q. Kaas, Blockade of neuronal α7-nAChR by α-conotoxin ImI explained by computational scanning and energy calculations, PLoS Comput. Biol. 7 (2011) e1002011. doi:10.1371/journal.pcbi.1002011.

[41] W. Kabsch, C. Sander, Dictionary of protein secondary structure: pattern recognition of hydrogen-bonded and geometrical features, Biopolymers. 22 (1983) 2577–2637. doi:10.1002/bip.360221211.

[42] R.J. Clark, H. Fischer, S.T. Nevin, D.J. Adams, D.J. Craik, The synthesis, structural characterization, and receptor specificity of the α-conotoxin Vc1.1, J. Biol. Chem. 281 (2006) 23254–23263. doi:10.1074/jbc.M604550200.

[43] D. Servent, H.L. Thanh, S. Antil, D. Bertrand, P.J. Corringer, J.P. Changeux, A. Ménez, Functional determinants by which snake and cone snail toxins block the α7 neuronal nicotinic acetylcholine receptors, J. Physiol. Paris. 92 (1998) 107–111. doi:10.1016/S0928-4257(98)80146-0.

[44] D. Everhart, G.E. Cartier, A. Malhotra, A.V. Gomes, J.M. McIntosh, C.W. Luetje, Determinants of potency on α-conotoxin MII, a peptide antagonist of neuronal nicotinic receptors, Biochemistry. 43 (2004) 2732–2737. doi:10.1021/bi036180h.

[45] Y. Wu, D. Zhangsun, X. Zhu, Q. Kaas, M. Zhangsun, P.J. Harvey, D.J. Craik, J.M. McIntosh, S. Luo, α-Conotoxin [S9A]TxID potently discriminates between α3β4 and α6/α3β4 nicotinic acetylcholine receptors, J. Med. Chem. 60 (2017) 5826–5833. doi:10.1021/acs.jmedchem.7b00546.

[46] M. Ellison, Z.-P. Feng, A.J. Park, X. Zhang, B.M. Olivera, J.M. McIntosh, R.S. Norton, α-RgIA, a novel conotoxin that blocks the α9α10 nAChR: structure and identification of key receptor-binding residues, J. Mol. Biol. 377 (2008) 1216–1227. doi:10.1016/j.jmb.2008.01.082.

[47] P.A. Quiram, S.M. Sine, Structural elements in α-conotoxin ImI essential for binding to neuronal α7 receptors, J. Biol. Chem. 273 (1998) 11007–11011. doi:10.1074/jbc.273.18.11007.

[48] A.J. Hone, M. Ruiz, M. Scadden, S. Christensen, J. Gajewiak, L. Azam, J.M. McIntosh, Positional scanning mutagenesis of α-conotoxin PeIA identifies critical residues that confer potency and selectivity for α6/α3β2β3 and α3β2 nicotinic acetylcholine receptors, J. Biol. Chem. 288 (2013) 25428–25439. doi:10.1074/jbc.M113.482059.

[49] L. Azam, U. Maskos, J.-P. Changeux, C.D. Dowell, S. Christensen, M. De Biasi, J.M. McIntosh, α-Conotoxin BuIA[T5A;P6O]: a novel ligand that discriminates between α6β4 and α6β2 nicotinic acetylcholine receptors and blocks nicotine-stimulated norepinephrine release, FASEB J. 24 (2010) 5113–5123. doi:10.1096/fj.10-166272.

[50] J.M. McIntosh, L. Azam, S. Staheli, C. Dowell, J.M. Lindstrom, A. Kuryatov, J.E. Garrett, M.J. Marks, P. Whiteaker, Analogs of α-conotoxin MII are selective for α6-containing nicotinic acetylcholine receptors, Mol. Pharmacol. 65 (2004) 944–952. doi:10.1124/mol.65.4.944.

[51] E.L. Millard, S.T. Nevin, M.L. Loughnan, A. Nicke, R.J. Clark, P.F. Alewood, R.J. Lewis, D.J. Adams, D.J. Craik, N.L. Daly, Inhibition of neuronal nicotinic acetylcholine receptor subtypes by α-conotoxin GID and analogues, J. Biol. Chem. 284 (2009) 4944–4951. doi:10.1074/jbc.M804950200.

[52] J. Banerjee, A.B. Yongye, Y.-P. Chang, R. Gyanda, J.L. Medina-Franco, C.J. Armishaw, Design and synthesis of α-conotoxin GID analogues as selective α4β2 nicotinic acetylcholine receptor antagonists, Biopolymers. 102 (2014) 78–87. doi:10.1002/bip.22413.

[53] P.H.N. Celie, I.E. Kasheverov, D.Y. Mordvintsev, R.C. Hogg, P. van Nierop, R. van Elk, S.E. van Rossum-Fikkert, M.N. Zhmak, D. Bertrand, V. Tsetlin, T.K. Sixma, A.B. Smit, Crystal structure of nicotinic acetylcholine receptor homolog AChBP in complex with an α-conotoxin PnIA variant, Nat. Struct. Mol. Biol. 12 (2005) 582–588. doi:10.1038/nsmb951.

[54] S. Dutertre, C. Ulens, R. Büttner, A. Fish, R. van Elk, Y. Kendel, G. Hopping, P.F. Alewood, C. Schroeder, A. Nicke, A.B. Smit, T.K. Sixma, R.J. Lewis, AChBP-targeted α-conotoxin correlates distinct binding orientations with nAChR subtype selectivity, EMBO J. 26 (2007) 3858–3867. doi:10.1038/sj.emboj.7601785.

[55] S.B. Hansen, G. Sulzenbacher, T. Huxford, P. Marchot, P. Taylor, Y. Bourne, Structures of Aplysia AChBP complexes with nicotinic agonists and antagonists reveal distinctive binding interfaces and conformations, EMBO J. 24 (2005) 3635–3646. doi:10.1038/sj.emboj.7600828.

[56] R.B. Jacobsen, R.G. DelaCruz, J.H. Grose, J.M. McIntosh, D. Yoshikami, B.M. Olivera, Critical residues influence the affinity and selectivity of α-conotoxin MI for nicotinic acetylcholine receptors, Biochemistry. 38 (1999) 13310–13315. doi:10.1021/bi9907476.

[57] R. Halai, R.J. Clark, S.T. Nevin, J.E. Jensen, D.J. Adams, D.J. Craik, Scanning mutagenesis of α-conotoxin Vc1.1 reveals residues crucial for activity at the α9α10 nicotinic acetylcholine receptor, J. Biol. Chem. 284 (2009) 20275–20284. doi:10.1074/jbc.M109.015339.

[58] A.-H. Jin, H. Brandstaetter, S.T. Nevin, C.C. Tan, R.J. Clark, D.J. Adams, P.F. Alewood, D.J. Craik, N.L. Daly, Structure of α-conotoxin BuIA: influences of disulfide connectivity on structural dynamics, BMC Struct. Biol. 7 (2007) 28. doi:10.1186/1472-6807-7-28.

[59] D.R. Groebe, W.R. Gray, S.N. Abramson, Determinants involved in the affinity of α-conotoxins GI and SI for the muscle subtype of nicotinic acetylcholine receptors, Biochemistry. 36 (1997) 6469–6474. doi:10.1021/bi970195w.

[60] S. Chhabra, A. Belgi, P. Bartels, B.J. van Lierop, S.D. Robinson, S.N. Kompella, A. Hung, B.P. Callaghan, D.J. Adams, A.J. Robinson, R.S. Norton, Dicarba analogues of α-conotoxin RgIA. Structure, stability, and activity at potential pain targets, J. Med. Chem. 57 (2014) 9933–9944. doi:10.1021/jm501126u.

Figure 1

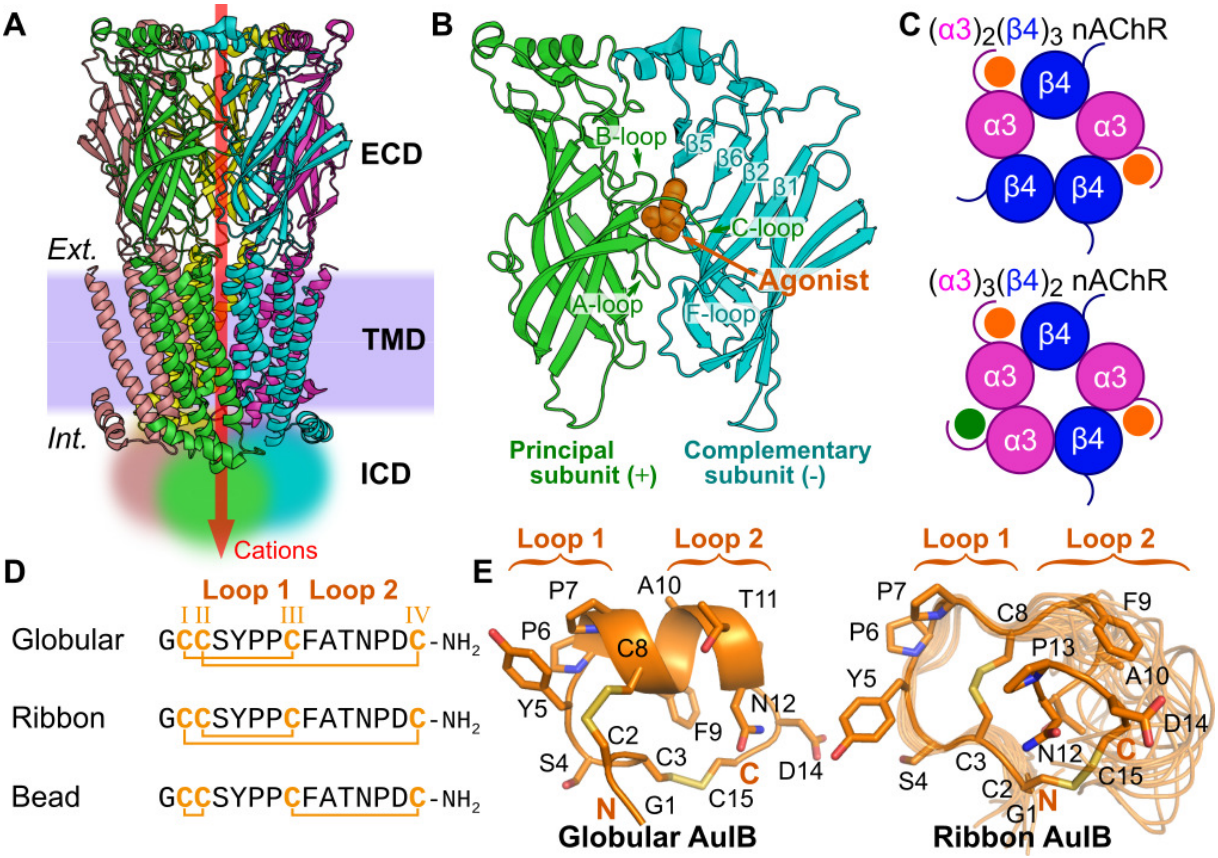
A
ECD
Ext.
TMD
Int.
ICD
Cations
B
B-loop
β5
β6
β2
β1
C-loop
Agonist
A-loop
F-loop
Principal subunit (+)
Complementary subunit (-)
C
(α3)2(β4)3 nAChR
β4
α3
α3
β4
β4
(α3)3(β4)2 nAChR
β4
α3
α3
α3
β4
D
Loop 1 Loop 2
I II III IV
Globular GCCSYPPCFATNPDC-NH2
Ribbon GCCSYPPCFATNPDC-NH2
Bead GCCSYPPCFATNPDC-NH2
E
Loop 1
Loop 2
P7
A10
T11
P6
C8
Y5
N12
C2
F9
S4
C3
C
D14
N
G1
C15
Globular AulB
Loop 1
Loop 2
P7
C8
F9
P6
P13
Y5
A10
D14
N12
C
S4
C3
C15
C2
N
G1
Ribbon AulB

Figure 2

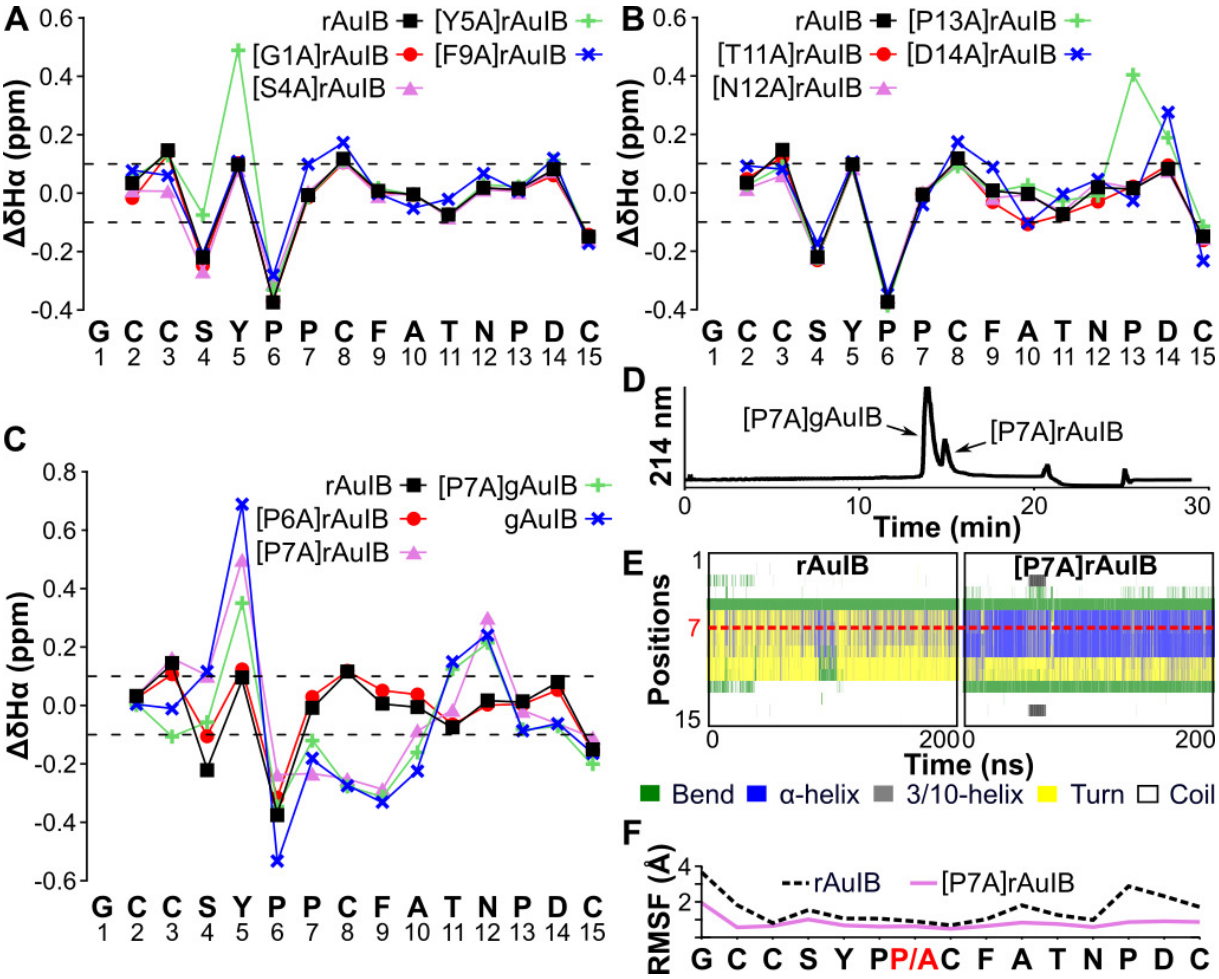
A
rAuIB
[Y5A]rAuIB
[G1A]rAuIB
[F9A]rAuIB
[S4A]rAuIB
ΔδHα (ppm)
G C C S Y P P C F A T N P D C
1 2 3 4 5 6 7 8 9 10 11 12 13 14 15
B
rAuIB
[P13A]rAuIB
[T11A]rAuIB
[D14A]rAuIB
[N12A]rAuIB
C
rAuIB
[P7A]gAuIB
[P6A]rAuIB
gAuIB
[P7A]rAuIB
D
214 nm
[P7A]gAuIB
[P7A]rAuIB
Time (min)
E
rAuIB
[P7A]rAuIB
Positions
Time (ns)
Bend
α-helix
3/10-helix
Turn
Coil
F
RMSF (Å)
rAuIB
[P7A]rAuIB
G C C S Y PP/AC F A T N P D C

Figure 3

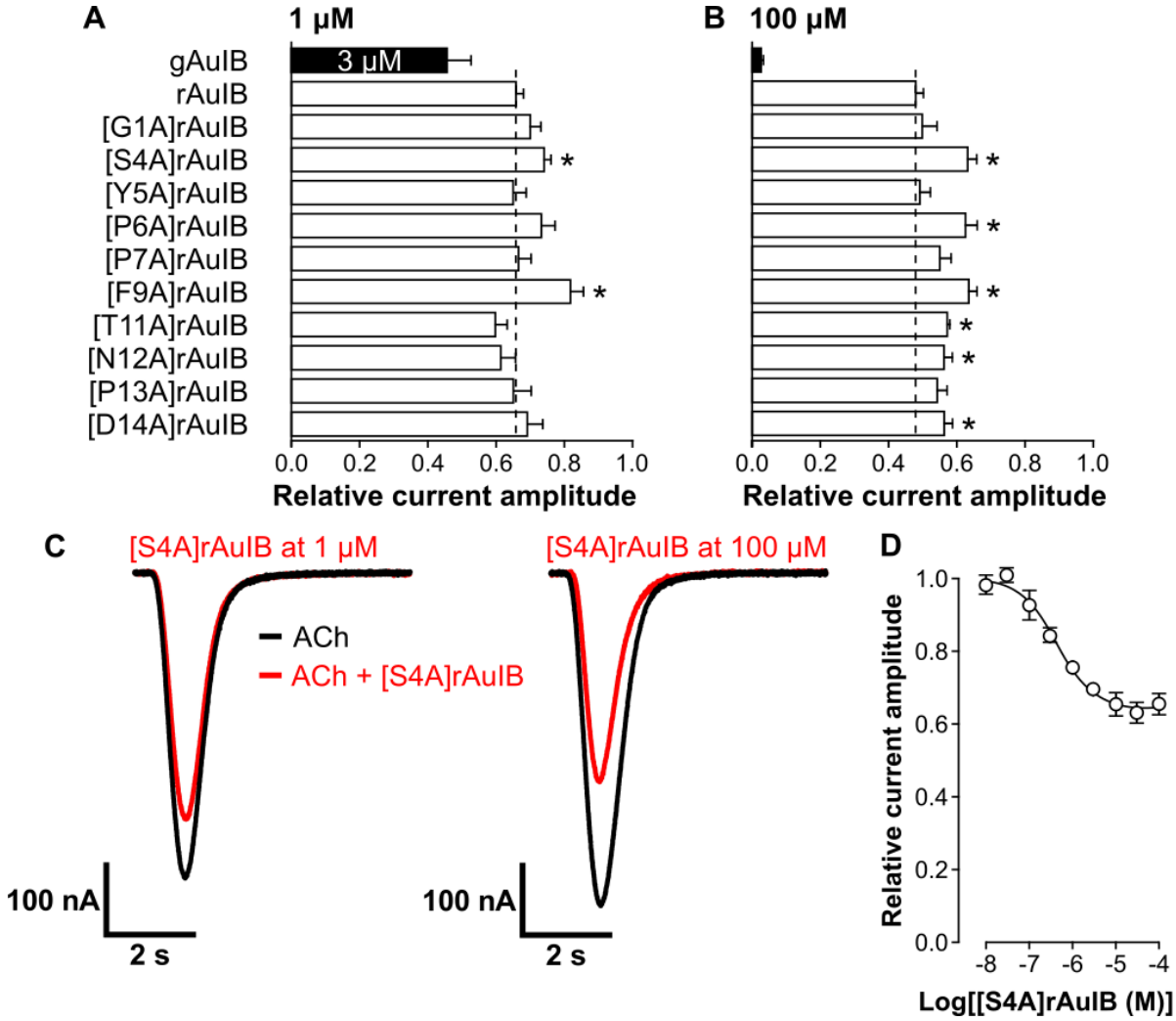
A
1 μM
3 μM
gAuIB
rAuIB
[G1A]rAuIB
[S4A]rAuIB
[Y5A]rAuIB
[P6A]rAuIB
[P7A]rAuIB
[F9A]rAuIB
[T11A]rAuIB
[N12A]rAuIB
[P13A]rAuIB
[D14A]rAuIB
0.0 0.2 0.4 0.6 0.8 1.0
Relative current amplitude
B
100 μM
0.0 0.2 0.4 0.6 0.8 1.0
Relative current amplitude
C
[S4A]rAuIB at 1 μM
ACh
ACh + [S4A]rAuIB
100 nA
2 s
[S4A]rAuIB at 100 μM
100 nA
2 s
D
Relative current amplitude
1.0
0.8
0.6
0.4
0.2
0.0
-8 -7 -6 -5 -4
Log[[S4A]rAuIB (M)]

Figure 4

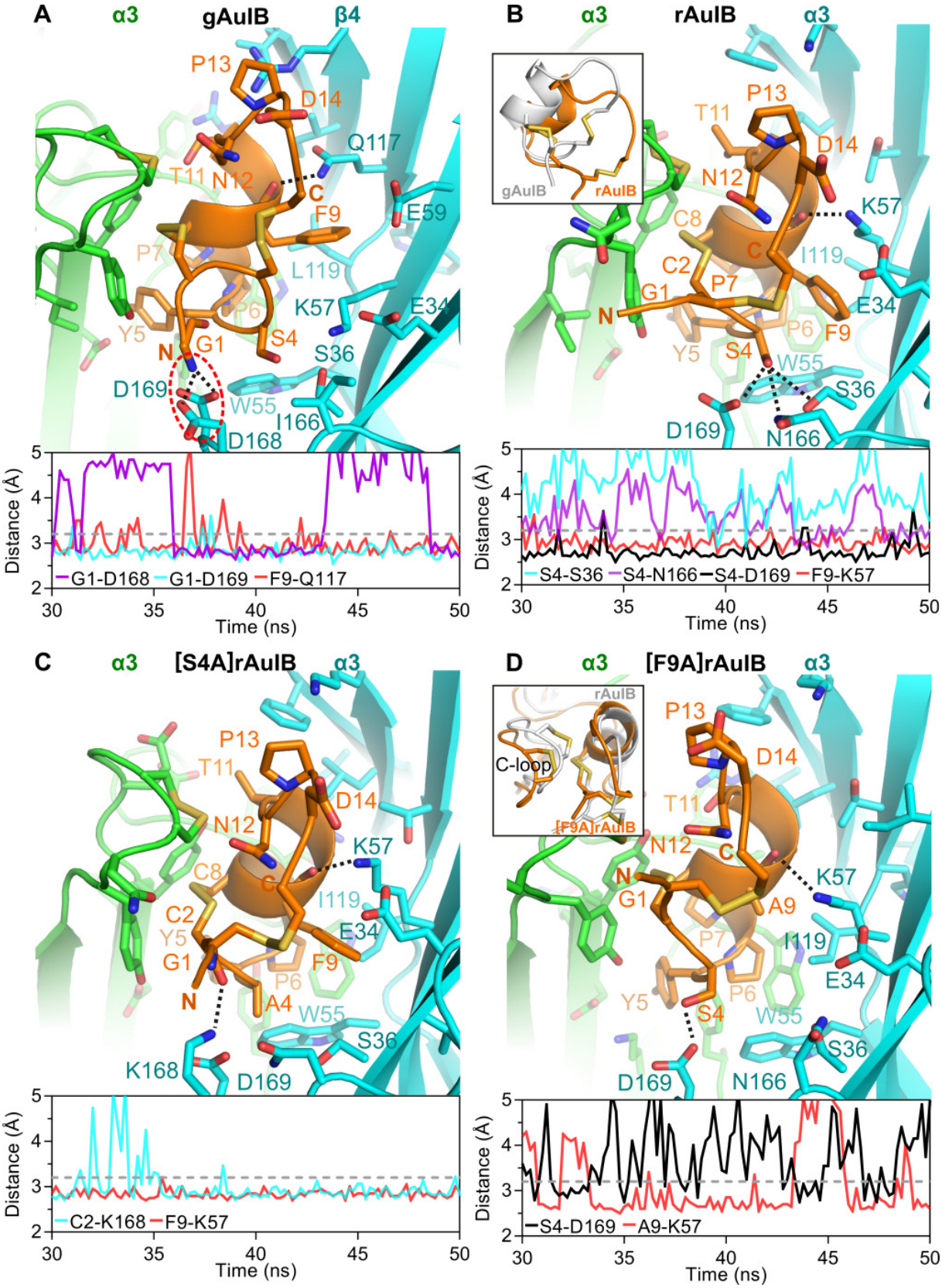
A
α3
gAulB
β4
P13
D14
Q117
T11
N12
C
F9
E59
P7
L119
P6
K57
E34
Y5
G1
S4
S36
N
D169
W55
I166
D168
Distance (Å)
G1-D168
G1-D169
F9-Q117
Time (ns)
B
α3
rAulB
α3
gAulB
rAulB
P13
T11
D14
N12
K57
C8
C
I119
C2
P7
G1
E34
N
P6
F9
Y5
S4
W55
S36
D169
N166
S4-S36
S4-N166
S4-D169
F9-K57
Time (ns)
C
α3
[S4A]rAulB
α3
P13
T11
D14
N12
K57
C8
C
I119
C2
E34
Y5
G1
P6
F9
N
A4
W55
S36
K168
D169
C2-K168
F9-K57
Time (ns)
D
α3
[F9A]rAulB
α3
rAulB
C-loop
[F9A]rAulB
P13
D14
T11
N12
C
K57
N
G1
A9
P7
I119
E34
Y5
P6
S4
W55
S36
D169
N166
S4-D169
A9-K57
Time (ns)

Figure legends

Fig. 1. Overview of the three-dimensional structure of nAChRs, the two main stoichiometries of α3β4 nAChRs, the three disulfide isomers of AuIB and the NMR spectroscopy solution structures of ribbon AuIB (rAuIB) and globular AuIB (gAuIB). A: The structure of nAChRs comprises three domains: an extracellular domain (ECD), a transmembrane domain (TMD), and an intracellular domain (ICD; ICD has not been resolved in the crystal structure). An arrow indicates the direction of cation movement through the central pore. The ribbon representation of the nAChR used the coordinates from the X-ray crystallography structure of the α4β2 nAChR (PDB: 5KXI). The membrane is represented by a purple rectangle and the extracellular (*Ext.*) and intracellular (*Int.*) sides of the membrane are indicated. B: Structure of the agonist binding site in the ECD, which is at the interface between a "principal" subunit (green) and a "complementary" subunit (cyan). The binding site is occupied by nicotine (orange). The ECD of each subunit displays one α-helix and 10 β-strands (β1 to β10), and the A-, B- , C- and F-loops are indicated. C: Illustration of the two main stoichiometries of homopentameric α3β4 nAChRs and identification of the functional binding sites. The illustration represents the nAChR as seen from the extracellular side and parallel to the membrane; the pore is in the center of the pentamer. The C-loop of each subunit is indicated by a curved line. The α3(+)β4(−) and α3(+)α3(−) agonist binding sites are indicated by orange and green discs, respectively. D: Amino acid sequence of the disulfide isomers of AuIB. Cys residues are numbered with Roman numerals (I–IV) and the disulfide bonds are shown as orange sticks. E: Three-dimensional NMR solution structures of gAuIB (PDB: 1MXN) and rAuIB (PDB: 1MXP).

Fig. 2. Secondary Hα chemical shifts (ΔδHα) of gAuIB, rAuIB and their variants (panels A, B and C) and analysis of the conformation of [P7A]rAuIB (panels D, E and F). A, B and C:

Secondary Hα chemical shifts of gAuIB, [P7A]gAuIB, rAuIB, and the rAuIB variants. The sequence of AuIB is indicated at the bottom. The dashed lines at 0.1 ppm and -0.1 ppm indicate the cut-off considered for assessing regular secondary structure content (above 0.1 ppm is β-strand and under -0.1 ppm is α-helix). D: Co-elution profile by reversed-phase HPLC of [P7A]rAuIB and [P7A]gAuIB monitored by absorbance at 214 nm. E: Secondary structure content of rAuIB and [P7A]rAuIB monitored over 200 ns molecular dynamics simulations. The positions in the sequence are on the y-axis. The secondary structure around position 7 is highlighted using a red dashed line. F: Root-mean-square fluctuation (RMSF) of the Cα of each position of rAuIB and [P7A]rAuIB over 200 ns molecular dynamics simulations. The RMSF was computed by fitting the Cα of the molecules to the first frame of each simulation.

Fig. 3. Activity of gAuIB, rAuIB and alanine mutants of rAuIB at the rat α3β4 nAChR. A and B: Bar graphs showing relative ACh-evoked peak current inhibition of rat α3β4 nAChR (α3:β4 = 10:1) by rAuIB analogues and gAuIB compared with rAuIB. In A, the peptides were tested at 1 μM, except gAuIB (3 μM). In B, the peptides were tested at 100 μM. The dashed lines indicate relative current amplitude in the presence of rAuIB. C: Superimposed representative traces of ACh-evoked currents mediated by rat α3β4 nAChR in the absence (black) and presence (red) of 1 μM (left) or 100 μM (right) [S4A]rAuIB. D: Concentration-response relationship of relative ACh-evoked current amplitude mediated by rat α3β4 nAChR (α3:β4 = 10:1) in the presence of [S4A]rAuIB (10 nM−100 μM) giving an IC_{50} of 441.8 ± 98.5 nM. Whole-cell currents at rat α3β4 were activated by 50 μM ACh. Relative current amplitude values are mean ± standard error of the mean; n = 5–9. The difference between the relative current amplitude of rAuIB and each variant was evaluated using the unpaired Student's t-test; * indicates a $p < 0.05$.

Fig. 4. Molecular models of complexes between α3β4 nAChR and gAuIB (A), rAuIB (B), [S4A]rAuIB (C), or [F9A]rAuIB (D). The evolution of a selection of distances indicative of hydrogen bonds between pairs of residues at the interface is shown at the bottom for each model. The α3(+) subunit is shown in green, the α3(−) or β4(−) subunit is shown in cyan, the peptides are shown in orange, and the disulfide bonds are shown in yellow. Hydrogen bonds monitored in the bottom panel are displayed as dotted black lines on the structure. Interactions between charged side chains are circled with a dotted red line. The distances were evaluated during the last 20 ns of each molecular dynamics simulation. The label for each distance comprises the residue of the toxin followed by the residue of the receptor. A dashed line at 3.2 Å indicates the upper-limit between the donor and acceptor atoms involved in a hydrogen bond. Panel B inset shows an overlay of the binding modes of rAuIB (orange) and gAuIB (white). Panel D inset shows that the C-loop in the [F9A]rAuIB molecular model (orange) moves outward compared to the C-loop in the model of the rAuIB/α3β4 nAChR complex (white).

Table 1. Amino acid sequences of gAuIB, rAuIB and variants synthesized and characterized in this study.

Peptide name	Sequence	Theoretical mass[a]	Observed mass[a]
gAuIB	GCCSYPPCFATNPDC-NH_2	1572.8	1572.2
rAuIB	GCCSYPPCFATNPDC-NH_2	1572.8	1572.4
[G1A]rAuIB	ACCSYPPCFATNPDC-NH_2	1586.8	1586.6
[S4A]rAuIB	GCCAYPPCFATNPDC-NH_2	1556.8	1556.6
[Y5A]rAuIB	GCCSAPPCFATNPDC-NH_2	1480.7	1480.3
[P6A]rAuIB	GCCSYAPCFATNPDC-NH_2	1546.7	1546.4
[P7A]rAuIB	GCCSYPACFATNPDC-NH_2	1546.7	1546.4
[F9A]rAuIB	GCCSYPPCAATNPDC-NH_2	1496.7	1496.3
[T11A]rAuIB	GCCSYPPCFAANPDC-NH_2	1542.8	1542.4
[N12A]rAuIB	GCCSYPPCFATAPDC-NH_2	1529.8	1529.4
[P13A]rAuIB	GCCSYPPCFATNADC-NH_2	1546.8	1546.4
[D14A]rAuIB	GCCSYPPCFATNPAC-NH_2	1528.8	1528.4
[P7A]gAuIB	GCCSYPACFATNPDC-NH_2	1546.7	1546.2

[a] Average mass in Dalton.